



HAL
open science

Study of oxygen reduction mechanism on Ag modified Sm_{1.8}Ce_{0.2}CuO₄ cathode for solid oxide fuel cell

Li-Ping Sun, Qiang Li, Hui Zhao, Li-Hua Huo, Jean-Paul Viricelle, Christophe Pijolat

► **To cite this version:**

Li-Ping Sun, Qiang Li, Hui Zhao, Li-Hua Huo, Jean-Paul Viricelle, et al.. Study of oxygen reduction mechanism on Ag modified Sm_{1.8}Ce_{0.2}CuO₄ cathode for solid oxide fuel cell. International Journal of Hydrogen Energy, 2013, 38 (32), pp.14060-14066. 10.1016/j.ijhydene.2013.08.069 . hal-00957382

HAL Id: hal-00957382

<https://hal.science/hal-00957382v1>

Submitted on 20 Mar 2014

HAL is a multi-disciplinary open access archive for the deposit and dissemination of scientific research documents, whether they are published or not. The documents may come from teaching and research institutions in France or abroad, or from public or private research centers.

L'archive ouverte pluridisciplinaire **HAL**, est destinée au dépôt et à la diffusion de documents scientifiques de niveau recherche, publiés ou non, émanant des établissements d'enseignement et de recherche français ou étrangers, des laboratoires publics ou privés.

1 **Study of oxygen reduction mechanism on Ag modified**
2 **Sm_{1.8}Ce_{0.2}CuO₄ cathode for solid oxide fuel cell**

3

4

5 **Li-Ping Sun¹ — Hui Zhao¹ — Qiang Li¹ — Li-Hua Huo¹ — Jean-Paul Viricelle*² —**
6 **Christophe Pijolat²**

7 ¹ Heilongjiang University, School of Chemistry and Materials Science, Key Laboratory of
8 Functional Inorganic Material Chemistry

9 ² Ecole Nationale Supérieure des Mines, SPIN-EMSE, PRESSIC, CNRS:UMR 5307, LGF, F-
10 42023 Saint-Etienne, France

11

12

13 * Corresponding author: Tel: +33 4 77 42 02 52

14 E-mail address: viricelle@emse.fr

15 **ABSTRACT**

16 Different amount of metal silver particles are infiltrated into porous $\text{Sm}_{1.8}\text{Ce}_{0.2}\text{CuO}_4$ (SCC)
17 scaffold to form SCC–Ag composite cathodes. The chemical stability, microstructure
18 evolution and electrochemical performance of the composite cathode are investigated using
19 X-ray diffraction (XRD), scanning electron microscopy (SEM), and AC impedance
20 spectroscopy respectively. The composite cathode exhibits enhanced chemical stability. The
21 metal Ag remains un-reacted with SCC and $\text{Ce}_{0.9}\text{Gd}_{0.1}\text{O}_{1.95}$ (CGO) at 800 °C for 72 h. The
22 polarization resistance of the composite cathode decreases with the addition of metal Ag. The
23 optimum cathode SCC-Ag05 exhibits the lowest area specific resistance (ASR, $0.43 \Omega \text{ cm}^2$) at
24 700 °C in air. Investigation shows that metal Ag accelerates the charge transfer process in the
25 composite cathode, and the rate limiting step for electrochemical oxygen reduction reaction
26 (ORR) changes to oxygen dissociation and diffusion process.

27 *KEYWORDS: Solid oxide fuel cell; Silver infiltration; Composite cathode; Electrode reaction*

28

29

30 **1 Introduction**

31 One of the research targets for SOFCs is lowering the operating temperature in order to
32 increase the life-time of the cell/stack/module as well as to reduce the cost of the materials. So
33 far, many studies have been focused on the development of new electrode and electrolyte
34 materials toward low temperature operable SOFCs [1], [2], [3] and [4]. Layered perovskite
35 oxides with K_2NiF_4 -type structure were extensively studied in recent years, due to their
36 promising transport and catalytic properties, thermochemical stability and compatibility with
37 other cell components [5], [6], [7], [8], [9], [10], [11], [12], [13], [14] and [15]. Among these
38 oxides, Ln_2CuO_4 materials were found to exhibit excellent performance. For example, Li et
39 al. reported that the ASR of the $La_{1.7}Sr_{0.3}CuO_4$ cathode was as low as $0.16 \Omega \text{ cm}^2$ at $700 \text{ }^\circ\text{C}$
40 [16]. We studied the electrochemical performance of $Sm_{2-x}Ce_xCuO_4$ and the ASR of
41 $Sm_{1.8}Ce_{0.2}CuO_4$ was found to be $1.16 \Omega \text{ cm}^2$ at $700 \text{ }^\circ\text{C}$ [17]. Further research on the oxygen
42 reduction kinetics of these cuprate cathodes always found that the charge transfer reaction was
43 the rate limiting step [16], [17], [18], [19] and [20]. Thus, enhancing the oxygen reduction
44 activity of these cathode materials is crucial for the development of novel IT-SOFC cathode.

45

46 Studies proved that cathodes infiltrated with Palladium (Pd) and platinum (Pt) metal particles
47 showed promising oxygen reduction activity, due to the substantially increase of the surface
48 catalysis properties [21] and [22]. Ag is another attractive infiltrating candidate than those
49 precious metals, due to its good catalytic activity, high electrical conductivity and relatively
50 low cost. Numerous works have been performed on the Ag-added perovskite cathodes [23],
51 [24], [25], [26] and [27], but less attention was paid to the K_2NiF_4 -type material [28].

52

53 To continue our studies on $\text{Sm}_{1.8}\text{Ce}_{0.2}\text{CuO}_4$ (referred as SCC in this paper) cathode materials,
54 and to understand the effect of Ag doping on the electrode performance, SCC-Ag composite
55 cathode was selected and the electrochemical property was studied compared with the bare
56 SCC electrode. The mechanism of the oxygen reduction on the SCC-Ag composite cathode
57 was investigated using electrochemical impedance spectroscopy (EIS) technique.

58 **2 Experimental**

59 $\text{Sm}_{1.8}\text{Ce}_{0.2}\text{CuO}_4$ powder was synthesized using the glycine-nitrate process (GNP). According
60 to the formula, stoichiometric amount of metal nitrates were mixed in a beaker to form a
61 solution, and then glycine (aminoacetic acid, $\text{H}_2\text{NCH}_2\text{CO}_2\text{H}$) was added into the nitrate
62 solution at 1:2 M ratio of metal ions/glycine according to propellant chemistry. After drying
63 and firing, the resultant powder was calcined in air at 1000 °C for 12 h. The $\text{Ce}_{0.9}\text{Gd}_{0.1}\text{O}_{1.95}$
64 (CGO) powder (Rhodia Courbevoie, France) was pressed uniaxially at 220 MPa and sintered
65 at 1400 °C for 10 h to form a densified pellet. In order to perform EIS measurement, a test
66 cell with three electrodes configuration was constructed. The $\text{Sm}_{1.8}\text{Ce}_{0.2}\text{CuO}_4$ powder was
67 mixed with terpineol to form a slurry, and subsequently painted on one side of the CGO
68 electrolyte pellet to form an electrode area of 0.5 cm², used as working electrode (WE). The
69 WE was first heated at 400 °C for 2 h to eliminate organic binders, followed by sintering at
70 1000 °C for 4 h in air, with a heating/cooling rate of 3 °C min⁻¹. Platinum paste was painted
71 on the other side of the CGO pellet in symmetric configuration, and then sintered at 800 °C
72 for 1 h in air, to form porous counter electrode (CE). A Pt wire was used as reference
73 electrode (RE) and put on the same side of the working electrode. Silver nitrate solution was
74 then infiltrated into the porous cathode. The detail of infiltration process was as follows: 0.05
75 mol L⁻¹ AgNO_3 solution was prepared by dissolving silver nitrate powders in mixture solution
76 of distilled water and ethanol. Ethanol was added to reduce the surface tension on SCC

77 backbone. The ratio of ethanol to water is 1 to 1. The infiltration was carried out in a vacuum
78 chamber by dripping the AgNO_3 solution onto the SCC cathode area carefully using an
79 injector and drying at $80\text{ }^\circ\text{C}$. The infiltrated cathode was then calcined at $800\text{ }^\circ\text{C}$ for one hour.
80 This infiltration step was repeated several times to obtain a suitable weight of Ag loaded on
81 the SCC backbone. The obtained cathodes with different weight ratio of Ag were abbreviated
82 as SCC-Ag02 for $\text{Sm}_{1.8}\text{Ce}_{0.2}\text{CuO}_4$ with 2 wt.% Ag, SCC-Ag05 for $\text{Sm}_{1.8}\text{Ce}_{0.2}\text{CuO}_4$ with 5
83 wt.% Ag, and so on.

84

85 In order to check the chemical stability of SCC with CGO at high temperature, these two
86 components were mixed thoroughly in 1:1 weight ratio, and heat-treated at $1000\text{ }^\circ\text{C}$ for 4 h in
87 air. Silver nitrate was then added to the mixture, and again heated up to $800\text{ }^\circ\text{C}$ for 72 h to
88 form SCC–CGO–Ag composite powders.

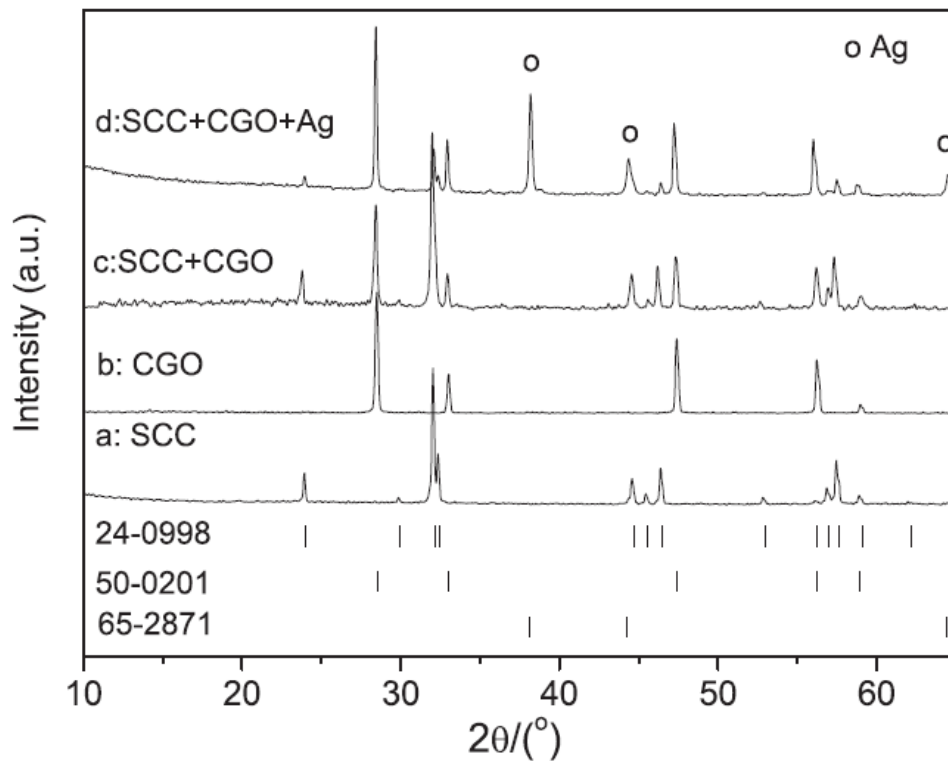
89

90 The sample was characterized using X-ray diffraction instrument (Rigaku, D/MAX-3B) and
91 scanning electron microscopy (SEM) (Hitachi, S-4700 FEG), respectively. The impedance
92 spectra were recorded over the frequency range 1 MHz to 0.1 Hz using Autolab PGStat30.
93 The measurements were performed at OCV as a function of temperature ($550\text{--}700\text{ }^\circ\text{C}$) and
94 oxygen partial pressure (in N_2/O_2 mixed atmosphere).

95 **3 Results and discussion**

96 Phase purity of the prepared SCC and chemical compatibility of Ag metal with SCC and
97 CGO were first investigated. Fig. 1 shows XRD patterns of the sintered SCC–CGO and SCC–
98 CGO–Ag composite powders. The spectra of pure SCC and CGO materials are also presented
99 in the same figure for comparison. The SCC powder made by GNP process crystallizes in
100 body-centered tetragonal symmetry (Fig. 1(a)), consisting with Sm_2CuO_4 structure (PDF card

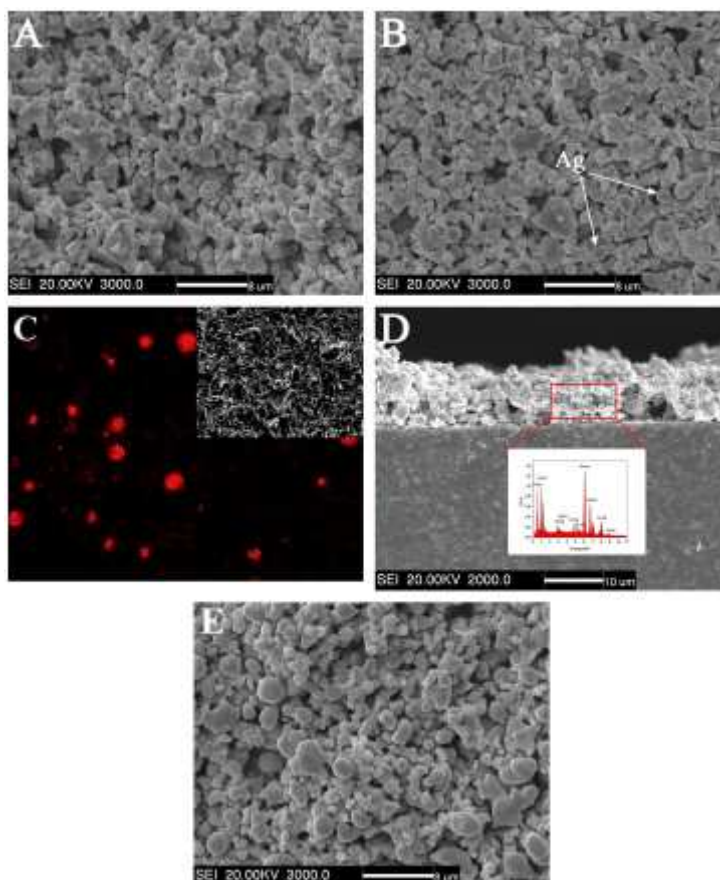
101 No. 24-0998). After sintered at 1000 °C for 4 h, SCC and CGO retained their own structures
102 in the SCC–CGO mixture (Fig. 1(c)). When Ag was added and the composite cathode was
103 then heated at 800 °C for prolonged 72 h, no additional peaks except those from metal Ag,
104 SCC and CGO can be detected (Fig. 1(d)). This result indicates that Ag is highly chemical
105 compatible with SCC and CGO materials.



106
107 Fig. 1: XRD patterns of SCC, CGO, SCC–CGO and SCC–CGO–Ag powders.

108 The SEM images of SCC and SCC–Ag cathodes are comparably shown in Fig. 2. Obviously a
109 fine microstructure with moderate porosity and well-necked particles is formed in the SCC
110 cathode after firing at 1000 °C for 4 h (Fig. 2(A)). The impregnation of Ag does not change
111 the microstructure adversely. Some round-shape particles are found in the SCC-Ag05 cathode
112 after the infiltration of AgNO₃ and then firing at 800 °C for 1 h (Fig. 2(B)). The surface
113 mapping result indicates that these round-shape particles are metallic Ag, which are dispersed
114 uniformly on the surface of the cathode (Fig. 2(C)). The average particle size of Ag is about
115 1–2 μm. The cross-sectional image of the SCC-Ag05 cathode and the CGO electrolyte is

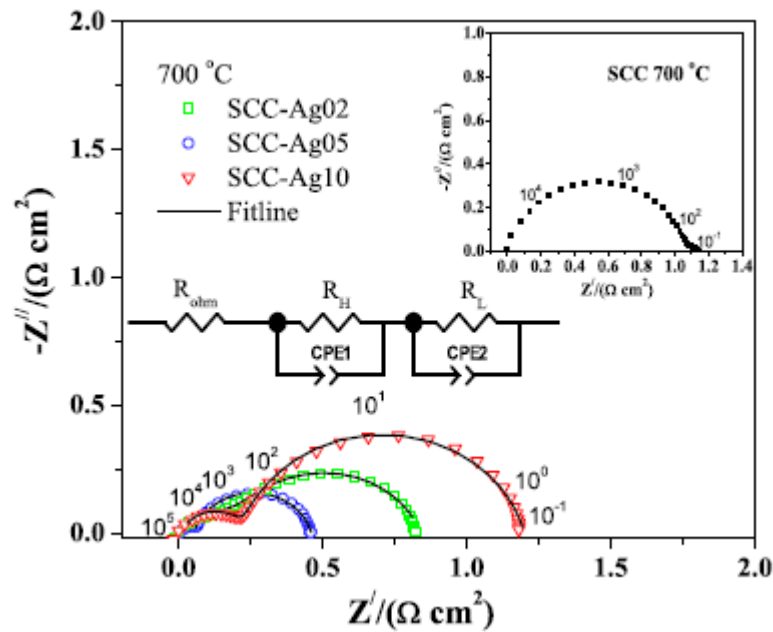
116 presented in Fig. 2(D). Clearly the cathode and the electrolyte form good contact with each
117 other. There is no delamination or cracking that can be observed at the electrode/electrolyte
118 interface. The thickness of the electrode is about 15 μm (Fig. 2(D)). The EDX result further
119 supports that metal Ag is distributed in the SCC-Ag05 cathode (Fig. 2(D), inset). When the
120 Ag loading increases to 10 wt.%, however, the glomeration and growth of Ag particles can be
121 visualized (Fig. 2(E)). This aggregation results in less TPBs and thus can be suspected to increase
122 the polarization resistance.



123
124 Fig. 2: SEM micrographs of the cathodes: (A) SCC without Ag (1000 $^{\circ}\text{C}$, surface), (B) SCC-
125 Ag05 (800 $^{\circ}\text{C}$, surface), (C) EDS elemental Mapping to show the spatial distribution of
126 metallic Ag (red), inset shows the mapping area of SCC-Ag05 cathode: (D) SCC-Ag05 (800
127 $^{\circ}\text{C}$, cross-sectional image), inset is the EDX result of the cross-sectional part of SCC-Ag05
128 cathode, (E) SCC with 10 wt.% Ag (800 $^{\circ}\text{C}$, surface).

129 To explore the effects of Ag loading on polarization resistance, the impedance spectra of SCC
130 cathode impregnated with different amounts of Ag were measured (Fig. 3). For all the
131 cathodes, the impedance spectra can be separated into two arcs located in the high-frequency
132 zone and the low-frequency zone respectively, implying two consecutive reaction processes
133 related to oxygen reduction reaction (ORR) might take place. The overall size of the two arcs
134 is primarily attributed to the cathode area specific resistance (ASR), which is widely used to
135 describe the resistance terms related to electrode process. The Arrhenius plots of ASR are
136 given in Fig. 4. Obviously the activation energy (E_a) of SCC–Ag cathode is much smaller
137 than SCC cathode. The ASR decreases with the Ag content, reaches a minimum at 5 wt.%
138 Ag, and then increases again at 10 wt.% Ag. The variation of ASR with Ag contents can be
139 understood, considering that the ORR process of the SCC electrode is likely promoted by the
140 surface modification with silver. However, with the further increase of Ag content in the
141 composite cathode, some surface of the SCC particles may be covered by the Ag metal, and
142 the active sites for oxygen reduction reaction will be reduced. This deduction was proved by
143 fitting the impedance spectra with an equivalent circuit (Fig. 3, inset) composed of two R-
144 CPE elements in series to obtain the resistance of different processes. In this equivalent
145 circuit, R_{ohm} represents the combination of electrolyte resistance, electrode ohmic resistance,
146 lead resistance and contact resistance between cathode and Pt mesh current collector, R_H and
147 R_L are the polarization resistance (R_p) corresponding to the high-frequency and low-frequency
148 arc, respectively. The ASR is the sum of R_H and R_L . CPE is constant phase element whose
149 value reflects the reaction mechanism of different electrode processes. The fitting results are
150 presented in Fig. 5. It can be seen that R_H is much larger than R_L in SCC cathode. In a
151 previous study, we proved that the reaction rate limiting step of SCC cathode was charge
152 transfer reaction, which was characterized by the high frequency arc in the EIS spectrum [17].
153 Compared to SCC electrode, the addition of Ag reduces dramatically the value of ASR and

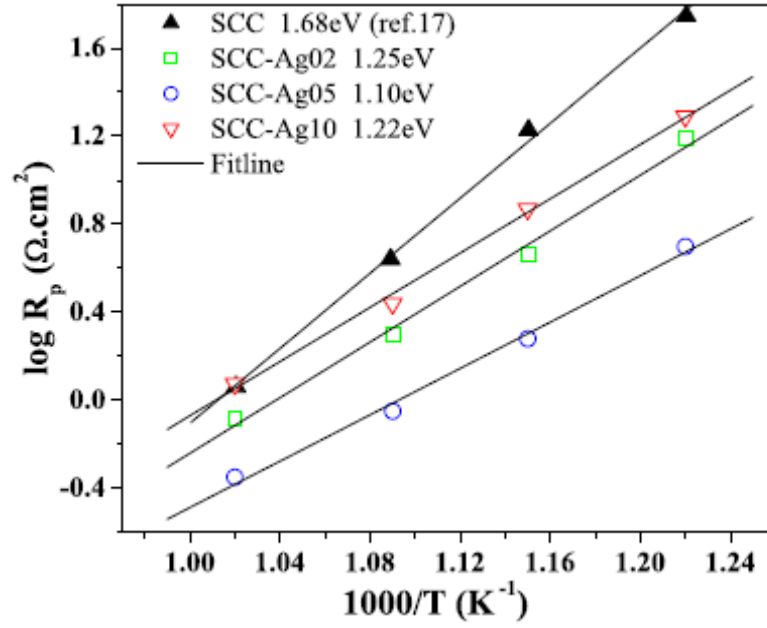
154 the decrease is mainly attributed by the reduction of R_H . Arrhenius plots of the fitting results
 155 for SCC–Ag composite cathode are given in Fig. 6. It is found that both R_H and R_L first
 156 decreases with the addition of Ag, and then increases again when the Ag content is up to 10
 157 wt.% in the SCC–Ag composite. The activation energy for R_H is in the range of 1.52–1.55 eV,
 158 close to the activation energy of the oxygen surface exchange process in $\text{La}_2\text{NiO}_{4+\delta}$ [5]. At the
 159 same time, the low frequency arc becomes dominant in the impedance spectra (Fig. 3), and
 160 the values of R_L are larger than these of R_H in the SCC–Ag composite cathodes (Fig. 6). The
 161 activation energy for R_L is in the range of 0.96–1.16 eV, which is close to the dissociation and
 162 diffusion activation energy of the adsorbed oxygen molecular on the cathode surface [29].
 163 The contribution of Ag loading is further illustrated in the Bold plot (Fig. 7). The enhanced
 164 charge transfer reaction can be seen by a dramatic decrease of the phase angle of the high
 165 frequency peak in the Bold plot. This is clearly different from that of SCC cathode. According
 166 to the fitting results, this difference indicates that the oxygen reduction mechanism has been
 167 changed with the addition of Ag.



168

169

Fig. 3: Nyquist plot for SCC–Ag composite cathodes measured at 700 °C in air.

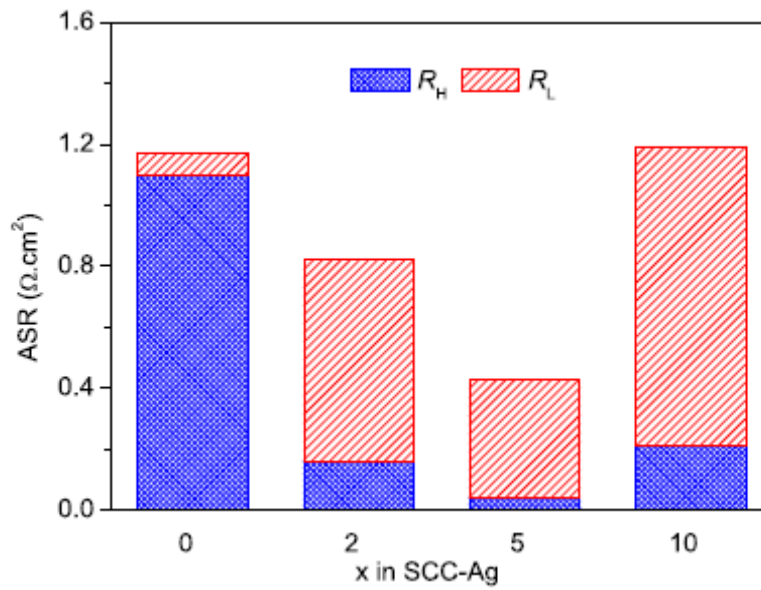


170

171

Fig. 4: Temperature dependence of the polarization resistance R_p for various SCC-xAg composites measured in air.

172

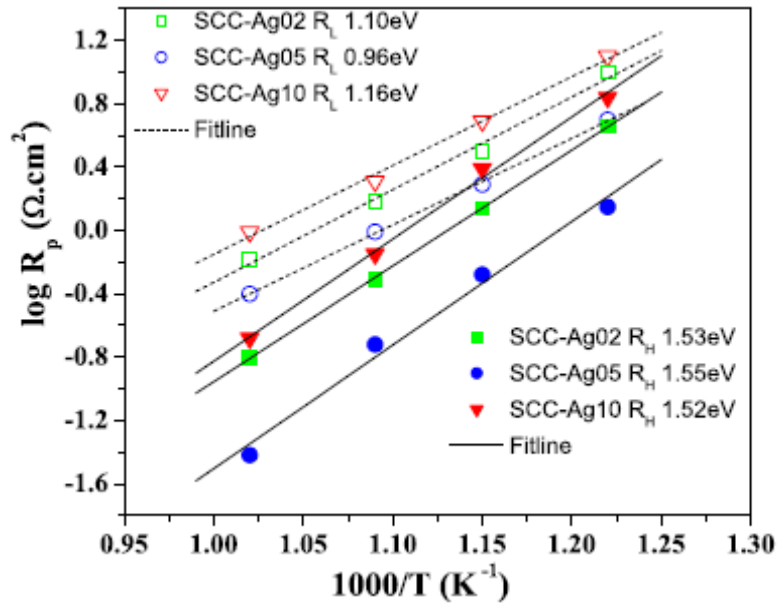


173

174

Fig. 5: Comparative evolution of the polarization resistance (R_H and R_L) with different amount of Ag in the SCC-Ag composite cathode.

175



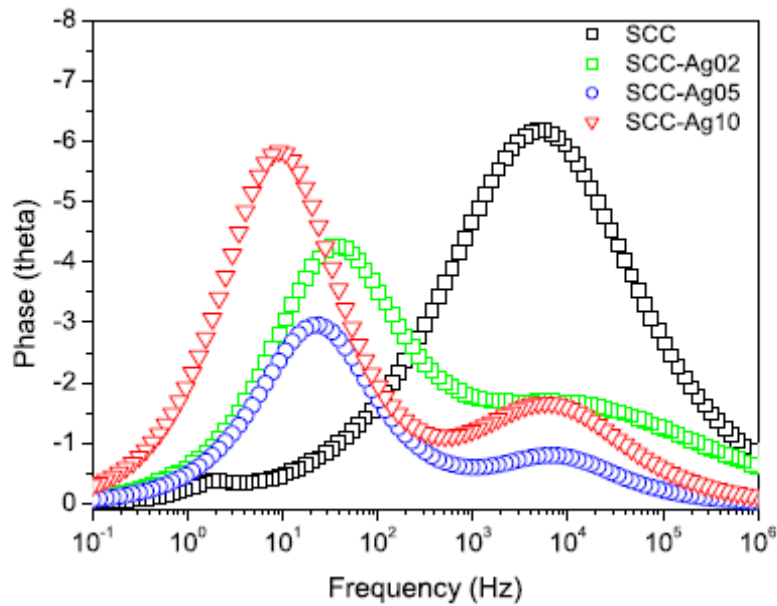
176

177

Fig. 6: Temperature dependences of fitted high frequency resistances and low frequency

178

resistances of the SCC–Ag composite electrodes with different Ag content.



179

180

Fig. 7: Bode plot for SCC–Ag composite cathodes measured at 700 °C in air.

181

The electrochemical reaction mechanism of SCC–Ag composite cathode was studied as a

182

function of oxygen partial pressure. Fig. 8 shows the impedance spectra of SCC-Ag05

183

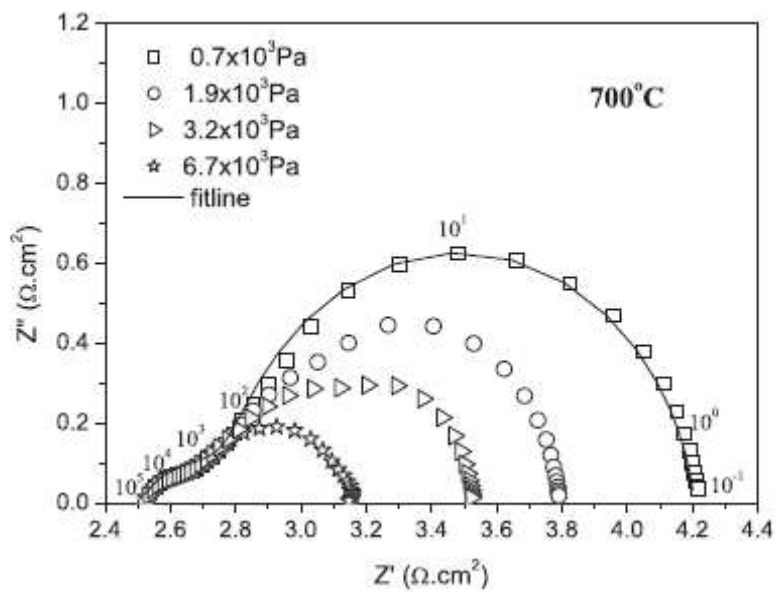
cathode measured at 700 °C under various oxygen partial pressures (P_{O_2}). The polarization

184

resistance decreases with the increase of oxygen partial pressure, indicating an oxygen

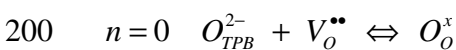
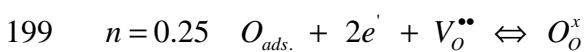
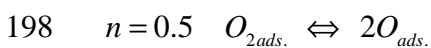
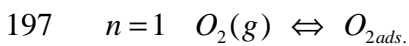
185 activity related electrochemical reaction that occurred on the composite cathode. By using the
 186 same equivalent circuit presented in Fig. 3, the values of R_H and R_L under different oxygen
 187 partial pressure can be calculated. It is found that the resistance of the high frequency arc (R_H)
 188 is always much smaller than that of the low frequency one (R_L). This means that the R_L related
 189 process is the reaction rate limiting step. Generally, the polarization resistance (R_p) varies
 190 with the oxygen partial pressure according to the following equation:

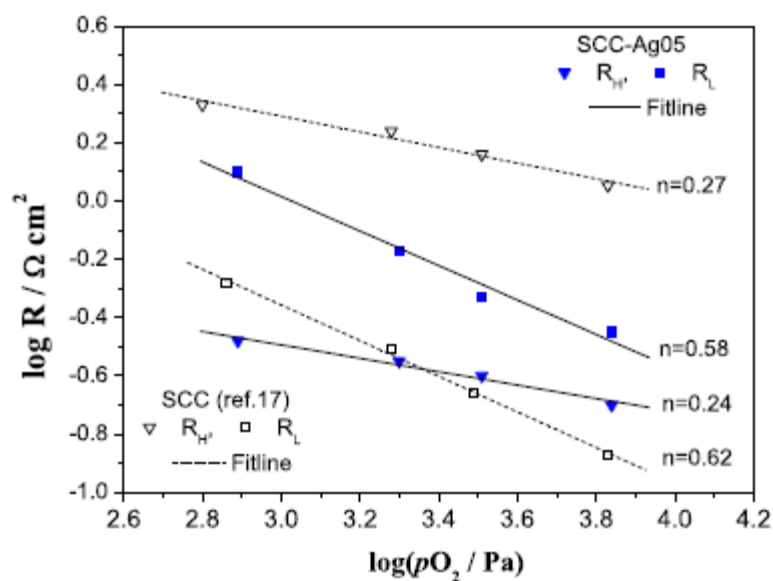
191
$$R_p = R_p^0 \times (P_{O_2})^n$$



192
 193 Fig. 8: Impedance spectra for the SCC-Ag05 cathode on CGO at 700 °C under various
 194 oxygen partial pressures.

195 The value of n could give useful information about the type of species involved in the
 196 reactions [30] and [31]:





201

202 Fig. 9: Dependence of polarization resistance on oxygen partial pressure for SCC-Ag05

203 composite cathode at 700 °C.

204 The dependence of polarization resistances (R_H and R_L , respectively) on oxygen partial was

205 presented in Fig. 9. It is found that the values of n corresponding to R_H and R_L are 0.24 and

206 0.58 respectively. In this case the high frequency arc is confirmed to be related to the charge

207 transfer process, and the low frequency arc is assigned to the dissociation and diffusion of

208 adsorbed oxygen. Compared to the results obtained in Fig. 8, it is clear that the R_L related

209 process is the major rate limiting step for SCC-Ag05 composite cathode in the whole range of

210 measurement oxygen partial pressure. However for SCC cathode, the n values of R_H and R_L

211 are 0.27 and 0.62 respectively, and the value of R_H is always larger than R_L , which implied

212 that the charge transfer process on SCC cathode is the rate limiting step [17]. So it is clear that

213 when Ag was added in the electrode, a change of the rate limiting step from charge transfer

214 process to diffusion of the dissociative adsorbed oxygen was likely happened. As we

215 expected, Ag catalyst promotes the surface exchange process (charge transfer reaction) and

216 additionally, Ag particles can provide additional electron transport pathway through the

217 cathode surface due to its high electronic conductivity. Therefore, the oxygen reduction

218 reaction could be more effective at the boundary of Air/Ag/SCC than at Air/SCC, and

219 consequently the electrochemical performance is enhanced by the impregnation of Ag
220 catalyst.

221 It should point out that the great reduce of R_H value is paid back by the simultaneous increase
222 of R_L (Fig. 5). It is proposed that this simple infiltration method used may lead to the growth
223 of micrometer size Ag particles, which will cover the SCC particle surface and block the
224 oxygen diffusion channel in the cathode. So the microstructure of the cathode need to be
225 further optimized.

226 **4 Conclusion**

227 The $\text{Sm}_{1.8}\text{Ce}_{0.2}\text{CuO}_4\text{-Ag}$ composite cathodes were prepared and their electrochemical
228 properties were studied below 700 °C. The SCC-Ag05 composite exhibits improved catalytic
229 activity for the oxygen reduction reaction compared to the $\text{Sm}_{1.8}\text{Ce}_{0.2}\text{CuO}_4$ cathode, due to the
230 increased electronic conductivity and electro-catalytic activity contributed by Ag particles.
231 The lowest area specific resistance obtained at 700 °C in air is $0.43 \Omega \text{ cm}^2$ for SCC-Ag05
232 composite cathode. The addition of Ag in the SCC electrode changes the rate limiting step
233 from charge transfer process to oxygen dissociation and diffusion process. However, further
234 long-term stability investigation by operating over an extended period may be needed to
235 verify the effect of Ag diffusion.

236 **Acknowledgments**

237 This work was supported by National Natural Science Foundation of China (51072048,
238 51102083), Natural Science Foundation of Heilongjiang Province (JC201211, B201107),
239 Program for Science and Technology Project of Heilongjiang Province (WB10A204).

240

241 **References**

- 242 [1] D. Brett, A. Atkinson, N.P. Brandon, S.J. Skinner, Intermediate temperature solid oxide
243 fuel cells, *Chem Soc Rev*, 37 (2008), pp. 1568–1578
- 244 [2] B.C.H. Steele, A. Heinzl, Materials for fuel-cell technologies, *Nature*, 414 (2001), pp.
245 345–352
- 246 [3] C. Xia, Y. Li, Y. Tian, Q. Liu, Y. Zhao, L. Jia et al., A high performance composite ionic
247 conducting electrolyte for intermediate temperature fuel cell and evidence for ternary ionic
248 conduction, *J Power Sources*, 188 (2009), pp. 156–162
- 249 [4] W. Zhou, Z.P. Shao, Z.G. Liang, Z.H. Zhu, W.Q. Jin, N.P. Xu, A new cathode for solid
250 oxide fuel cells capable of in situ electrochemical regeneration, *J Mater Chem*, 21 (2011), pp.
- 251 [5] S.J. Skinner, J.A. Kilner, Oxygen diffusion and surface exchange in $\text{La}_{2-x}\text{Sr}_x\text{NiO}_{4+\delta}$, *Solid*
252 *State Ionics*, 135 (2000), pp. 709–712
- 253 [6] V.V. Kharton, A. Viskup, E. Naumovich, F. Marques, Oxygen ion transport in La_2NiO_4 -
254 based ceramics, *J Mater Chem*, 9 (1999), pp. 2623–2629
- 255 [7] A. Hernández, L. Moggi, A. Caneiro, $\text{La}_{2-x}\text{Sr}_x\text{NiO}_{4+\delta}$ as cathode for SOFC: reactivity
256 study with YSZ and CGO electrolytes, *Int J Hydrogen Energy*, 35 (2010), pp. 6031–6036

- 257 [8] J. Huang, R. Gao, Z. Mao, J. Feng, Investigation of $\text{La}_{2-x}\text{Sr}_x\text{NiO}_{4+\delta}$ based cathodes for
258 SDC -carbonate composite electrolyte intermediate temperature fuel cells, *Int J Hydrogen*
259 *Energy*, 35 (2010), pp. 2657–2662
- 260 [9] M.A. Daroukh, V.V. Vashook, H. Ullmann, F. Tietzb, I.A. Raj, Oxides of the AMO_3 and
261 A_2MO_4 - type: structural stability, electrical conductivity and thermal expansion, *Solid State*
262 *Ionics*, 158 (2003), pp. 141–150
- 263 [10] Y.S. Wang, H.W. Nie, S.R. Wang, T.L. Wen, U. Guth, V. Valshook, $\text{A}_{2-\alpha}\text{A}'_{\alpha}\text{BO}_4$ -type
264 oxides as cathode materials for IT-SOFCs ($\text{A} = \text{Pr, Sm}$; $\text{A}' = \text{Sr}$; $\text{B} = \text{Fe, Co}$), *Mater Lett*, 60
265 (2006), pp. 1174–1178
- 266 [11] H. Zhao, F. Mauvy, C. Lalanne, J.M. Bassat, S. Fourcade, J.C. Grenier, New cathode
267 materials for ITSOFC: phase stability oxygen exchange and cathode properties of
268 $\text{La}_{2-x}\text{NiO}_{4+\delta}$, *Solid State Ionics*, 179 (2008), pp. 2000–2005
- 269 [12] F. Mauvy, C. Lalanne, J.M. Bassat, J.C. Grenier, H. Zhao, P. Dordor *et al.*, Oxygen
270 reduction on porous $\text{Ln}_2\text{NiO}_{4+\delta}$ electrodes, *J Eur Ceram Soc*, 25 (2005), pp. 2669–2672
- 271 [13] L.P. Sun, Q. Li, L.H. Huo, H. Zhao, G.Y. Zhang, N. Lin *et al.*, Synthesis and
272 performance of $\text{Sr}_{1.5}\text{La}_x\text{MnO}_4$ as cathode materials for intermediate temperature solid oxide
273 fuel cell, *J Power Sources*, 196 (2011), pp. 5835–5839
- 274 [14] J. Dailly, S. Fourcade, A. Largeteau, F. Mauvy, J. Grenier, M. Marrony, Perovskite and
275 A_2MO_4 -type oxides as new cathode materials for protonic solid oxide fuel cells, *Electrochim*
276 *Acta*, 55 (2010), pp. 5847–5853

- 277 [15] G. Taillades, J. Dailly, M. Taillades-Jacquín, F. Mauvy, A. Essouhmi, M. Marrony *et al.*,
278 Intermediate temperature anode-supported fuel cell based on $\text{BaCe}_{0.9}\text{Y}_{0.1}\text{O}_3$ electrolyte with
279 novel Pr_2NiO_4 cathode, *Fuel Cells*, 10 (2010), pp. 166–173
- 280 [16] Q. Li, H. Zhao, L.H. Huo, L.P. Sun, X.L. Cheng, J.C. Grenier, Electrode properties of Sr
281 doped La_2CuO_4 as new cathode material for intermediate-temperature SOFCs, *Electrochem*
282 *Commun*, 9 (2007), pp. 1508–1512
- 283 [17] L.P. Sun, L.H. Huo, H. Zhao, Synthesis and performance of $\text{Sm}_{2-x}\text{Ce}_x\text{CuO}_4$ cathode
284 materials for IT-SOFC, *Chin J Inorg Chem*, 23 (2007), pp. 1545–1549
- 285 [18] Q. Li, X. Zeng, L.P. Sun, H. Zhao, L.H. Huo, J.C. Grenier, Electrochemical performance
286 of $\text{La}_2\text{Cu}_{1-x}\text{Co}_x\text{O}_4$ cathode materials for intermediate- temperature SOFCs, *Int J Hydrogen*
287 *Energy*, 37 (2012), pp. 2552–2558
- 288 [19] J.H. Hao, Q. Li, L.P. Sun, H. Zhao, L.H. Huo, Synthesis and performance of
289 $\text{Nd}_{2-x}\text{Sr}_x\text{CuO}_4$ cathode materials for IT-SOFC, *Chin J Inorg Chem*, 25 (2009), pp. 1818–1822
- 290 [20] L.P. Sun, H. Zhao, Q. Li, L.H. Huo, J.P. Viricelle, C. Pijolat, Study on $\text{Sm}_{1.8}\text{Ce}_{0.2}\text{CuO}_4$ -
291 $\text{Ce}_{0.9}\text{Gd}_{0.1}\text{O}_{1.95}$ composite cathode materials for intermediate temperature solid oxide fuel cell,
292 *Int J Hydrogen Energy*, 36 (2011), pp. 12555–12560
- 293 [21] H.J. Hwang, J.W. Moon, S. Lee, E.A. Lee, Electrochemical performance of LSCF-based
294 composite cathodes for intermediate temperature SOFCs, *J Power Sources*, 145 (2005), pp.
295 243–248

- 296 [22] T.J. Huang, X.D. Shen, C.L. Chou, Characterization of Cu, Ag and Pt added
297 $\text{La}_{0.6}\text{Sr}_{0.2}\text{Co}_{0.2}\text{Fe}_{0.8}\text{O}_{3-\delta}$ and gadolinia-doped ceria as solid oxide fuel cell electrodes by
298 temperature-programmed techniques, *J Power Sources*, 187 (2009), pp. 348–355
- 299 [23] Y. Lin, R. Ran, Z. Shao, Silver-modified $\text{Ba}_{0.5}\text{Sr}_{0.5}\text{Co}_{0.8}\text{Fe}_{0.2}\text{O}_{3-\delta}$ as cathodes for a proton
300 conducting solid-oxide fuel cell, *Int J Hydrogen Energy*, 35 (2010), pp. 8281–8288
- 301 [24] Y. Sakito, A. Hirano, N. Imanishi, Y. Takeda, O. Yamamoto, Y. Liu, Silver infiltrated
302 cathodes for intermediate temperature solid oxide fuel cells, *J Power Sources*, 182 (2008), pp.
303 476–481
- 304 [25] I. Wilkinson, J. Zhu, Ag-perovskite composite materials for SOFC cathode-interconnect
305 contact, *J Electrochem Soc*, 156 (2009), pp. B905–B912
- 306 [26] T. Suzuki, Y. Takahashi, K. Hanamoto, T. Yamaguchi, Y. Fujishiro, Low temperature
307 processed composite cathodes for solid-oxide fuel cells, *Int J Hydrogen Energy*, 36 (2011),
308 pp. 10998–11003
- 309 [27] T.J. Huang, C.L. Chou, Oxygen dissociation and interfacial transfer rate on performance
310 of SOFCs with metal-added $(\text{LaSr})(\text{CoFe})\text{O}_3-(\text{Ce, Gd})\text{O}_{2-\delta}$ cathodes, *Fuel Cells*, 10 (2010),
311 pp. 718–725
- 312 [28] Q. Li, L.P. Sun, L.H. Huo, H. Zhao, J. Grenier, Electrochemical performance of
313 $\text{La}_{1.6}\text{Sr}_{0.4}\text{NiO}_4$ - Ag composite cathodes for intermediate-temperature solid oxide fuel cells, *J*
314 *Power Sources*, 196 (2011), pp. 1712–1716

- 315 [29] Y.P. Yin, B.W. Liu, J.J. Qi, Y.S. Gu, Q.L. Liao, Z. Qin *et al.*, Characterization of
316 $\text{Ba}_{1.0}\text{Sr}_{1.0}\text{FeO}_{4+\delta}$ cathode on $\text{La}_{0.9}\text{Sr}_{0.1}\text{Ga}_{0.8}\text{Mg}_{0.2}\text{O}_{3-\delta}$ electrolyte for intermediate temperature
317 solid oxide fuel cells, *J Power Sources*, 196 (2011), pp. 6238–6241
- 318 [30] G. Zhan, X.M. Liu, B. Bergman, Z. Zhao, Investigation of oxygen reduction reaction
319 kinetics on $\text{Sm}_{0.5}\text{Sr}_{0.5}\text{CoO}_{3-\delta}$ cathode supported on $\text{Ce}_{0.85}\text{Sm}_{0.075}\text{Nd}_{0.075}\text{O}_{2-\delta}$ electrolyte,
320 *J Power Sources*, 196 (2011), pp. 9195–9203
- 321 [31] J.D. Kim, G.D. Kim, J.W. Moon, Y. Park, W.H. Lee, K. Kobayashi *et al.*,
322 Characterization of LSM-YSZ composite electrode by ac impedance spectroscopy, *Solid*
323 *State Ionics*, 143 (2001), pp. 379–389